Effect of Perfluoroalkyl Chain Length on Synthesis and Film Formation of Fluorine-Containing Colloidal Dispersions

W. Reid Dreher, Anuradha Singh, and Marek W. Urban*

School of Polymers and High Performance Materials, Shelby F. Thames Polymer Science Research Center, Department of Polymer Science, The University of Southern Mississippi, Hattiesburg, Mississippi 39406

Received January 12, 2005; Revised Manuscript Received March 29, 2005

ABSTRACT: The development of a new family of colloidal dispersions that exhibit nonspherical shapes and are capable of forming stable polymeric dispersions and films is reported. Heptadecafluorodecyl methacrylate (FMA), heptadecafluorodecyl acrylate (FA), heptadecafluoro-1-decene (FD), heptafluorobutyl acrylate (FBA), and heptafluorobutyl methacrylate (FBMA) were copolymerized with methyl methacrylate (MMA) and *n*-butyl acrylate (nBA) monomers leading to the formation of stable colloidal dispersions that contain up to 8.5% (w/w) of F-containing polymer. Atomic force microscopy (AFM), attenuated total reflectance Fourier transform infrared (ATR FTIR) spectroscopy, and internal reflection infrared imaging (IRIRI) showed that the length of the perfluoroalkyl side chain in F-containing monomers is directly related to surface concentration levles in coalesced films. These studies also show that incorporation of each F-containing monomer generates surface properties with enhanced water repellency as well as significant decreases of the kinetic coefficient of friction.

Introduction

Recently, we reported[1] that the presence and combination of surfactants may serve as a vehicle for the aqueous synthesis of stable colloidal particles that contain up to 8.5% (w/w) of polymerized F-monomers. These studies showed that when phosphoric acid bis(tridecafluorooctyl) ester ammonium salt (FSP) and sodium dodecyl sulfate (SDS) were utilized in the presence of methyl methacrylate (MMA), *n*-butyl acrylate (nBA), and heptadecafluorodecyl methacrylate (FMA), a sufficient decrease in surface tension of the aqueous phase is achieved which facilitates a suitable environment allowing for increased diffusions of FMA during emulsion polymerization. The resulting colloidal particle morphologies consisted of two distinct phases, where MMA and nBA randomly polymerized forming spherical particles after which FMA polymerized onto the exterior of p-MMA/nBA colloidal particles generating nonspherical morphologies. The unique aspect of this approach was that the synthesis of colloidal particles containing fluoropolymers was accomplished using a classical emulsion polymerization approach without complex reaction setups, cosolvents, or other accessories.[2−27]

The current studies capitalize on this convenient synthetic approach utilizing monomer-starved conditions implemented during emulsion polymerization and focus on the development of colloidal particles containing methyl methacrylate (MMA), *n*-butyl acrylate (nBA), and a series of F-monomers. Specifically, we will examine the effect of the length of the CF_2 tail on particle morphologies as well as its effect on film formation, structure−property relationships, and surface macroscopic properties. For this reason, we prepared methyl methacrylate/*n*-butyl acrylate (MMA/nBA) colloidal dispersions in the presence of 8.5% (w/w) copolymer content of heptadecafluorodecyl methacrylate (FMA), heptadecafluorodecyl acrylate (FA), heptadecafluoro-1-decene (FD), heptafluorobutyl acrylate (FBA), and heptafluorobutyl methacrylate (FBMA).

* To whom all correspondence should be addressed.

Experimental Section

Methyl methacrylate (MMA), *n*-butyl acrylate (nBA), heptadecafluorodecyl methacrylate (FMA), heptadecafluorodecyl acrylate (FA), heptadecafluoro-1-decene (FD), heptafluorobutyl acrylate (FBA), heptafluorobutyl methacrylate (FBMA), potassium persulfate (KPS), phosphoric acid bis(tridecafluorooctyl) ester ammonium salt (FSP), and sodium dodecyl sulfate (SDS) were purchased from Aldrich Chemical Co. All colloidal dispersions were synthesized under monomer-starved conditions using a semicontinuous polymerization process in which all monomer and surfactants were dissolved in water and stirred under high agitation to produce a semistable preemulsion, after which 10% (w/w) of the preemulsion and 18% (w/w) of the initiator solution were injected into the reaction kettle containing 100 g of water. This process facilitates the seeding of the emulsion polymerization. The mixture was allowed to stir for 30 min for initiation reactions to occur. Upon initiating polymerization, the remaining preemulsion was fed continuously over 3.5 h while the initiator solution was fed over 4 h. Upon the completion of the initiator feed, polymerization was allowed to continue for another 5 h. Polymerization reactions were carried out in a 1 L reaction kettle equipped with a reflux condenser at 79 °C in a N_2 atmosphere under continuous agitation (300 rpm) using a Caframo BDC3030 digital stirrer.

The synthesized colloidal particles consisted of MMA, nBA, and the following F-containing monomers: FMA, FA, FD, FBMA, and FBA. The copolymer content of each F-containing monomer in the colloidal particles was 8.5% (w/w). The amount of F-monomer incorporated into colloidal particles was determined from the initial feed composition of the initial monomer mixture combined with the analysis of the solid content after synthesis. Such weight measurements combined with NMR analysis published earlier allow accurate determination of the copolymer content.[1]

Remaining concentrations of individual components are reported elsewhere.[1] Particle size measurements were obtained using a Microtrac UPA 250. Figure 1a illustrates the structure of each F-containing monomer, and Figure 1b displays the particle size along with the particle size distribution curve of each colloidal dispersion. Such prepared colloidal dispersions were cast on a poly(vinyl chloride) (PVC) substrate and allowed

10.1021/ma050070w CCC: $30.25
Published on Web 04/23/2005

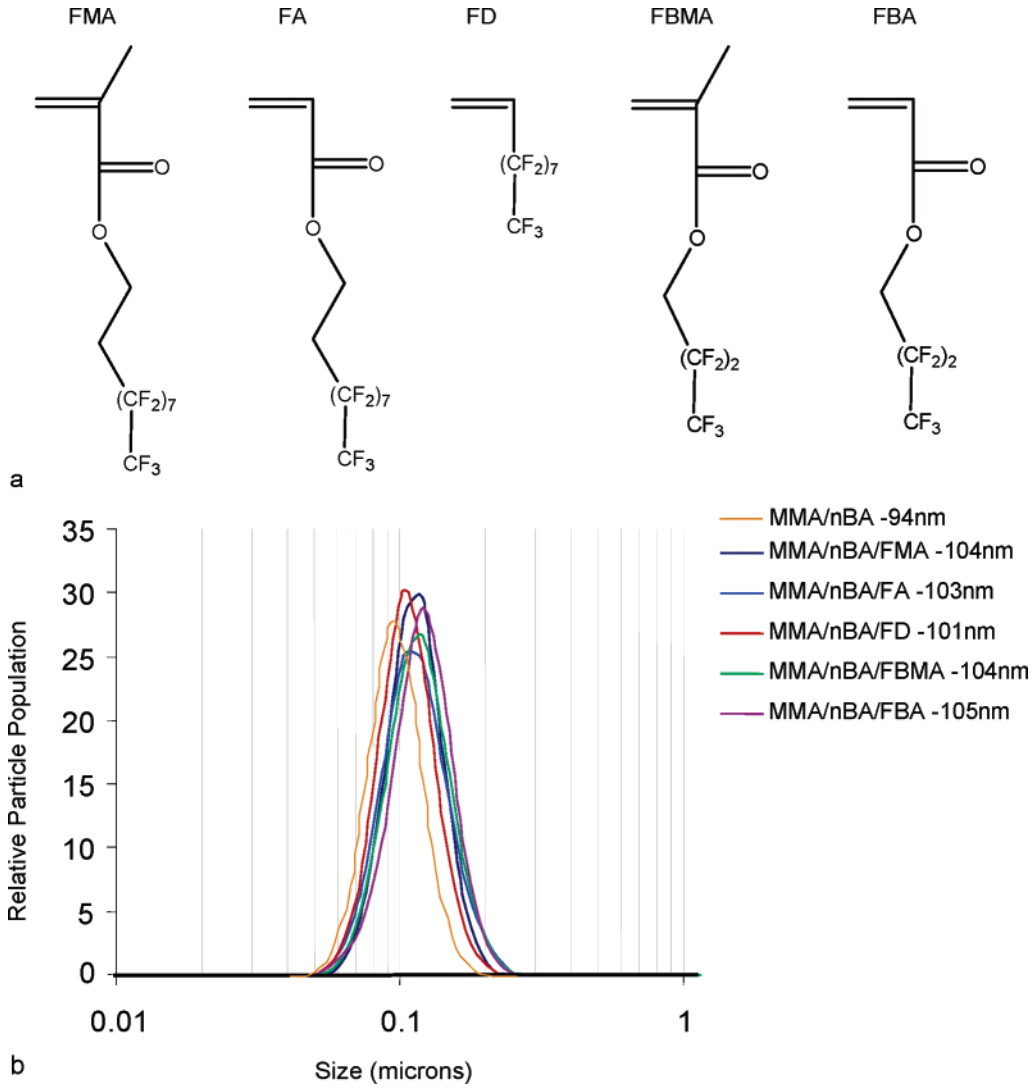

Figure 1. (a) Schematic representation of the F-monomers utilized during the synthesis of MMA/nBA/F-containing colloidal particles. (b) Particle size and particle size distribution curves for MMA/nBA, MMA/nBA/FMA, MMA/nBA/FA, MMA/nBA/FD, MMA/nBA/FBMA, and MMA/nBA/FBA.

to coalescence at 50% relative humidity (RH) for 3 days at 23 °C to form approximately 20 μm thick dry films. Film thickness was determined using a Pro Max caliper.

Polarized attenuated total reflectance Fourier transform infrared (ATR FTIR) spectra were collected using a Bio-Rad FTS-6000 FTIR single-beam spectrometer set at a 4 cm^{-1} resolution which was equipped with a ZnSe polarizer. A 45° face angle Ge crystal along with a ZnSe polarizer facilitates orientation studies by utilizing TE (transverse electric) and TM (transverse magnetic) modes of polarized IR light. Each spectrum represents 100 coadded scans ratioed against the same number of reference scans collected using an empty ATR cell. All spectra were corrected for spectral distortions and optical effects using Q-ATR software.[28,29]

Internal reflection infrared (IRIR) images were obtained using a Bio-Rad FTS 6000 Stingray system with a Ge internal reflection element (IRE). This system consists of a Bio-Rad FTS 6000 spectrometer, a UMA 500 microscope, an ImagIR focal plane array (FPA) image detector, and a semispherical germanium IRE. IRIR images were collected using the following spectral acquisition parameters: undersampling ratio = 4, step-scan speed = 2.5 Hz, number of spectrometer steps = 1777, number of images per step = 64, and spectral resolution = 8 cm^{-1}. As recent literature indicates,[30] the use of a Ge crystal in contact with the analyzed surface allows spatial resolution in the range of 1000 nm, thus overcoming spatial detection limits in the mid-IR. In a typical experiment, a spectral data set acquisition time was ≈15 min. Image processing was performed using ENVI (The Environment for Visualizing Images, Research Systems, Inc.) version 3.5. When necessary, baseline correction algorithims were used to compensate for a baseline drift.[30]

Thermal transitions were recorded using a TA Q800 dynamic mechanical analyzer (DMA) by heating the samples from −90 to 200 °C at a rate of 2 °C/min and at a frequency of 1 Hz. Atomic force microscopy phase images (Nanoscope IIIa Dimension 3000 scanning probe microscope, Digital Instruments) were obtained using a Si cantilever at a resonance frequency around 300 kHz.

Transmission electron micrographs (TEM) were acquired on a Zeiss EM 109T microscope using an accelerating voltage of 80 kV. Samples of colloidal dispersion used for TEM analysis were prepared by making a 1:10 000 dilution in deionized water followed by casting onto Formvar-coated copper grids (Ted Pella, Inc.).

Surface tension measurements of polymeric films were obtained using a FTA200 dynamic contact angle analyzer, and a Qualitest 1055 friction tester was utilized to determine the kinetic coefficient of friction.[31]

Results and Discussion

While Figure 1a illustrates chemical structures of F-monomers utilized in the synthesis of MMA/nBA colloidal particles, Figure 1b exhibits the results of particle size analysis. As seen, the particle sizes range

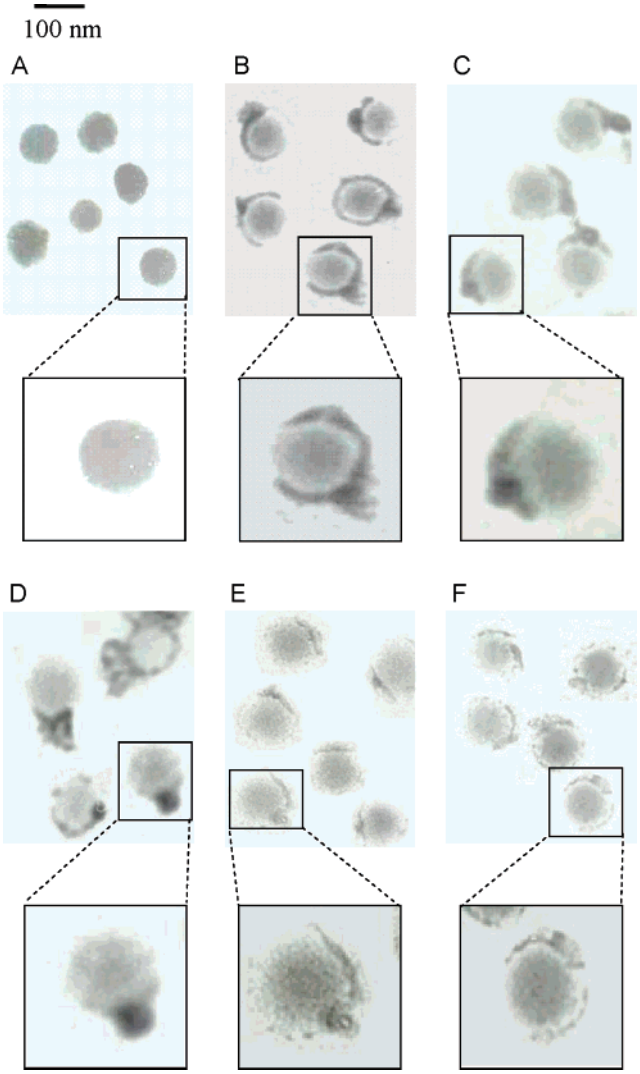

Figure 2. Transmission electron micrographs: (A) MMA/nBA, (B) MMA/nBA/FMA, (C) MMA/nBA/FA, (D) MMA/nBA/FD, (E) MMA/nBA/FBMA, and (F) MMA/nBA/FBA.

from 94 to 105 nm with monomodal distribution of the particles regardless of the F-monomer utilized. In an effort to identify particle morphologies, TEM images were collected, and Figure 2 illustrates TEM images of MMA/nBA (A), MMA/nBA/FMA (B), MMA/nBA/FA (C), MMA/nBA/FD (D), MMA/nBA/FBMA (E), and MMA/nBA/FBA (F). As shown in Figure 2A, MMA/nBA colloidal particles exist as monomodal entities with no considerable electron density changes, indicating a random copolymerization process. On the other hand, the presence of the long perfluoroalkyl side chains results in intraparticle phase separation with highly electron dense regions existing near the exterior of the particles (Figure 2B−D). These data also show that by decreasing the length of the perfluoroalkyl side chain, and as shown in Figure 2E,F, the size of the phase-separated entities within a particle decreases. These images reinforce the findings described in the previous studies,[1] thus confirming that an appropriate FSP/SDS surfactant combination facilitates the copolymerization of MMA/nBA/F-containing colloidal particles and that F-monomer polymerizes as a blocky, phase-separated entity onto the exterior of existing p-MMA/nBA colloidal particles. The latter was also confirmed by NMR measurements. As stated in the Experimental Section, each colloidal dispersion is capable of forming a stable colloidal film, but the question is how the presence of F-monomer copolymerized into MMA/nBA affects film properties as compared to MMA/nBA. We utilized DMA to obtain the storage modulus at temperatures below the T_g. The storage modulus of MMA/nBA is 615 MPa, whereas incorporation of 8.5% (w/w) FMA into MMA/nBA colloidal systems results in its increase to 850 MPa. This behavior is attributed to the rigid nature of the F-containing monomer.[32] Copolymerization of FA, FD, FBA, and FBMA into MMA/nBA colloidal particles also results in increased storage modules ranging from 720 to 900 MPa.

With these data in mind, it is of interest to elucidate how these differences affect surface macroscopic properties. For that purpose, we measured surface tension changes as well as the kinetic coefficients of friction at the F−A interface as a function of F-monomer, and these results are depicted in Figure 3. As seen, the presence of each copolymerized F-monomer alters the contact angle of a drop of water at the surface for each film, which for MMA/nBA/FMA is 100° and for MMA/nBA the contact agnle is 69°. Similarly, MMA/nBA/FA and MMA/nBA/FD exhibit contact angles of 96° and 101°, respectively. However, the contact angle for the shorter perfluoroalkyl side chained MMA/nBA/FBMA and MMA/nBA/FBA colloidal films decreases to about 90°. Although similar trends are observed for the kinetic coefficient of friction at the F−A interface, significantly

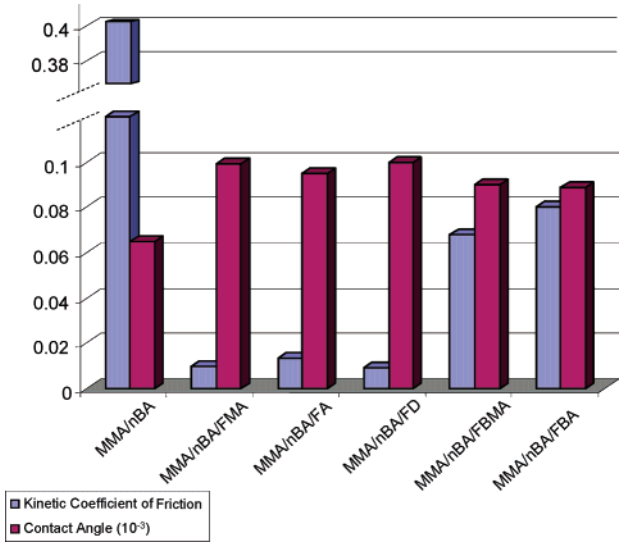

Figure 3. Kinetic coefficient of friction plotted as a function of colloidal composition. The same *y*-axis is also used to plot contact angle measurements (values should be multiplied by 1000).

lower values are observed for FMA, FA, and FD monomers. Similar to DMA experiments, longer perfluoroalkyl side chains produce surfaces with more polytetrafluoroethylene-like properties.

At this point, it is clear that the length of the CF_2 side chains affect both bulk and surface macroscopic measurements. The next question is what surface morphologies are responsible for these observed differences. Figure 4 illustrates a series of AFM phase images recorded from the F−A interface for MMA/nBA (A), MMA/nBA/FMA (B), MMA/nBA/FA (C), MMA/nBA/FD (D), MMA/nBA/FBMA (E), and MMA/nBA/FBA (F). Each image represents a 5 × 5 μm sample area. As shown, image A displays a continuous one-phase component attributed to p-MMA/nBA at the F−A interface, whereas image B (MMA/nBA/FMA) indicates the presence of high aspect ratio ordered entities at the F−A interface. Similar to previous studies,[1] the presence of the crystallites results from directional stratification near the F−A interface. For comparison, image C (MMA/nBA/FA) illustrates ordered domains of similar size and shape of FMA at the F−A interface, thus indicating similar surface properties between the $-(CF_2)_7-CF_3$ side chains of the acrylic and methacrylic F-monomers. On the other hand, the presence of the nonacrylic, vinyl F-monomer with a similar $-(CF_2)_7-CF_3$ side chain results in surface morphologies with increased size of the crystalline or mesophase domains at the F−A interface (image D). Images E and F of Figure 6 illustrate AFM images of MMA/nBA/FBMA and MMA/nBA/FBA, respectively. As shown, there is a significant decrease of the size and surface coverage of the heterogeneous domains as compared to images B−D, which is attributed to both FBMA and FBA possessing shorter perfluoroalkyl side chains ($-(CF_2)_2-CF_3$), subsequently leading to random aggregation with little to no crystalline components.[33−35] These data are consistent with earlier findings[10,36] which have shown that the formation of ordered domains of perfluoroalkyl side chains with FMA, FA, and FD can occur under ambient conditions, as displayed in images B−D.

Because of colloidal particles possessing F-containing moieties stratifying near the F−A interface as depicted in AFM Images, let us now elucidate their chemical information. For this, we utilized IRIRI in order to determine the chemical origin of the entities displayed

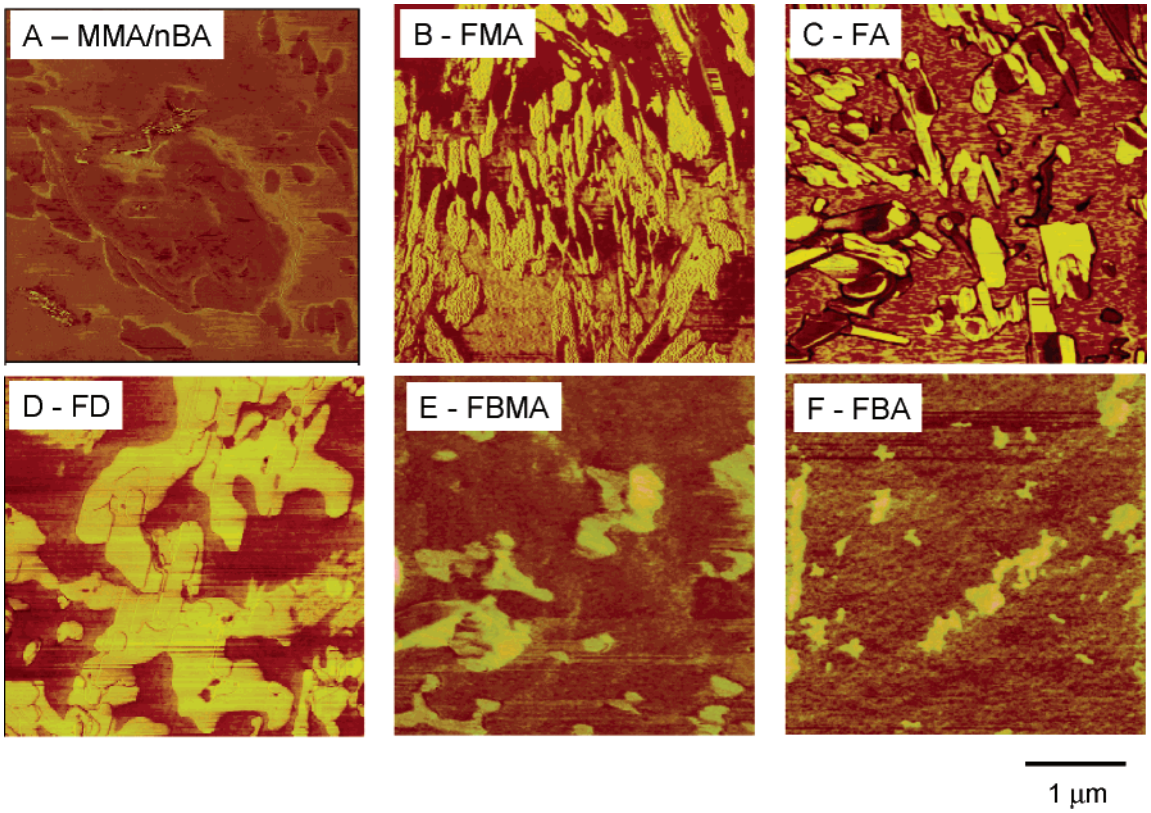

Figure 4. AFM phase images of copolymer films: (A) MMA/nBA, (B) MMA/nBA/FMA, (C) MMA/nBA/FA, (D) MMA/nBA/FD, (E) MMA/nBA/FBMA, and (F) MMA/nBA/FBA. Scan box for each image is 5 μm × 5 μm.

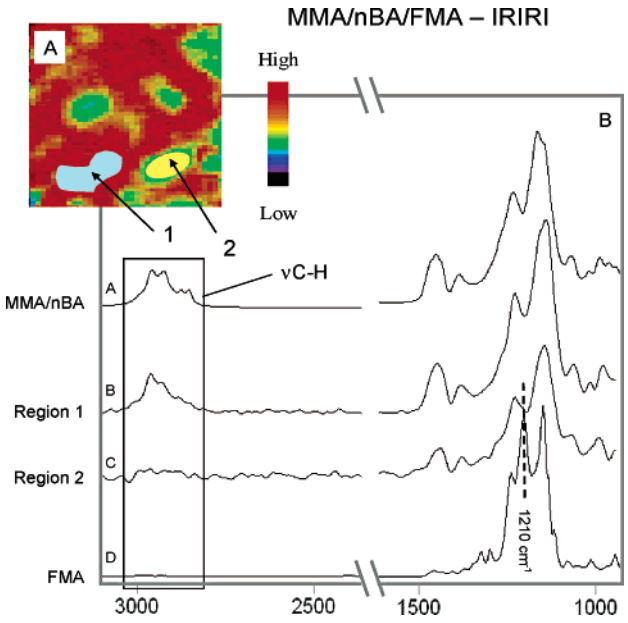

Figure 5. IRIR image recorded from the F−A interface of MMA/nBA/FMA colloidal films: (A) Image obtained by tuning into the 2945 cm^{-1} IR band. (B) IR spectra recorded from areas labeled 1 and 2 in (A). For reference purposes, IR spectra of MMA/nBA and FMA are included.

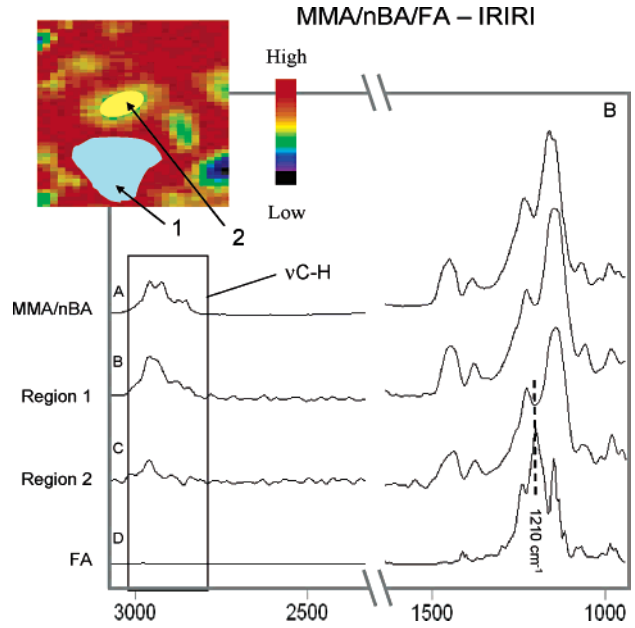

Figure 6. IRIR image recorded from the F−A interface of MMA/nBA/FA colloidal films: (A) Image obtained by tuning into the 2945 cm^{-1} IR band. (B) IR spectra recorded from areas labeled 1 and 2 in (A). For reference purposes, IR spectra of MMA/nBA and FA are included.

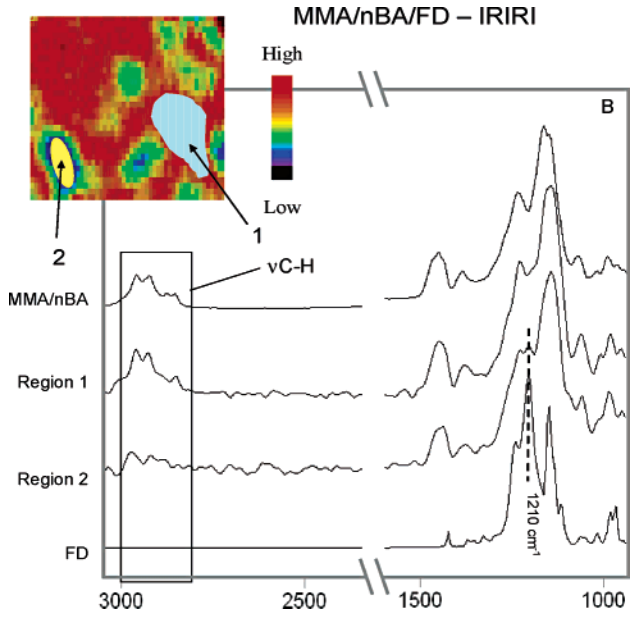

Figure 7. IRIR image recorded from the F−A interface of MMA/nBA/FD colloidal films: (A) Image obtained by tuning into the 2945 cm^{-1} IR band. (B) IR spectra recorded from areas labeled 1 and 2 in (A). For reference purposes, IR spectra of MMA/nBA and FD are included.

in the AFM Images. The results of these experiments are shown in Figures 6−9. Because of IRIRI experiments allowing for the tuning into a specific IR band associated with a given species, this method will be useful for determining areas prevalent with C−F entities. Figure 7A illustrates the IR image for MMA/nBA/FMA, which was produced by tuning into the 2924 cm^{-1} band. These results show that the C−H stretching vibrations of the copolymer matrix are detected, but their distribution is not uniform, thus resulting in a heterogeneous surface with regions consisting of significant reductions in concentration levels of the aliphatic $-CH_2$ moieties.

While the IR image in Figure 7A provides the spatial distribution of chemical entities near the surface, Figure 7B represents averaged IR information obtained from the regions labeled 1 and 2 in Figure 7A. As previously determined, region 1 is largely associated with the presence of aliphatic C−H groups, and in comparison to the IR spectrum of MMA/nBA, this area is attributed to p-MMA/nBA. Region 2 of Figure 7A represents an area on the surface generated through the absence of the 2945 cm^{-1} band, and the IR spectrum produced from this area shows an absence of C−H stretching vibrations and the presence of FMA. This is also manifested by the increased intensities of the 1210 cm^{-1} band due to C−F stretching vibrations.

The same analysis was performed on MMA/nBA/FA, MMA/nBA/FD, MMA/nBA/FBMA, and MMA/nBA/FBA films, and the results of these experiments are displayed

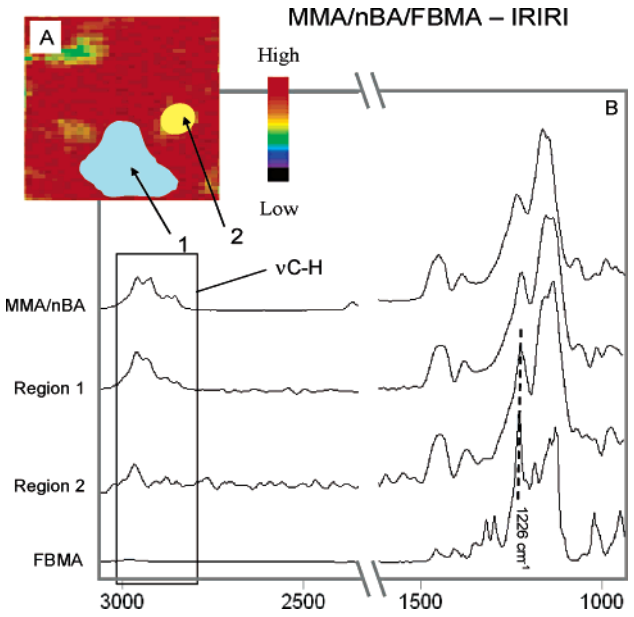

Figure 8. IRIR image recorded from the F−A interface of MMA/nBA/FBMA colloidal films: (A) Image obtained by tuning into the 2945 cm^{-1} IR band. (B) IR spectra recorded from areas labeled 1 and 2 in (A). For reference purposes, IR spectra of MMA/nBA and FBMA are included.

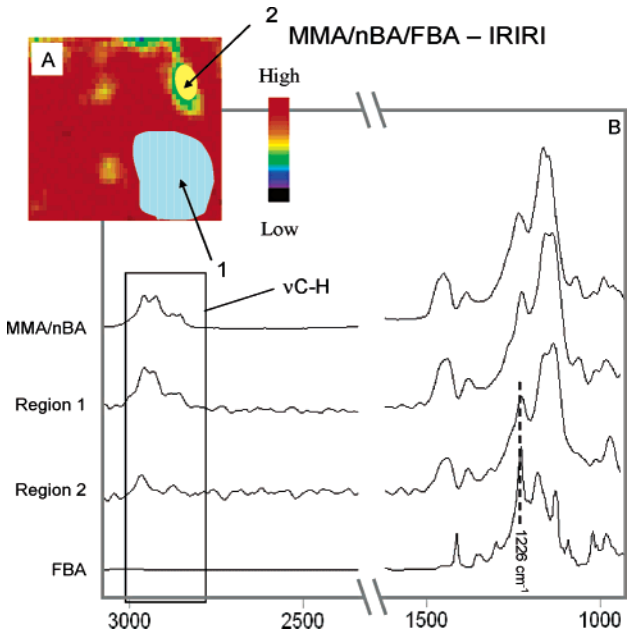

Figure 9. IRIR image recorded from the F−A interface of MMA/nBA/FBA colloidal films: (A) Image obtained by tuning into the 2945 cm^{-1} IR band. (B) IR spectra recorded from areas labeled 1 and 2 in (A). For reference purposes, IR spectra of MMA/nBA and FBA are included.

in Figures 6−9, respectively. These results are consistent with Figure 5 where, again, region 1 consists of MMA/nBA and region 2 consists of heterogeneous phase-separated entities consisting of high concentration levels of F-containing polymers. This is manifested by the spectra recorded from region 1 in Figures 6−9A, illustrating a p-MMA/nBA matrix with strong C−H functionality and region 2 which exhibits an absence of the 2945 cm^{-1} band and the presence of the C−F stretching vibrations for each F-containing monomer.

At this point, it should be noted that the phase-separated C−F regions in Figures 8 and 9 display a significant size decrease as compared to Figures 6 and 7. These results are consistent with the AFM data where MMA/nBA/FBMA and MMA/nBA/FBA films with shorter perfluoroalkyl side chains (Figure 5E,F) caused the decrease of both size and surface concentration levels of the crystalline domains.

Scheme 1. Pictorial Representation of the Processes Leading to Surface Phase-Separated Domains at the F−A Interface in the Presence of F-Containing Colloidal Particles

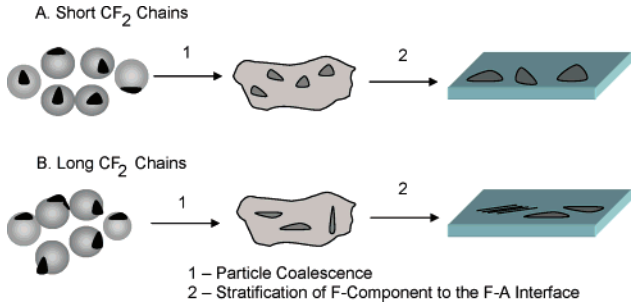

The primary driving force for F-containing species to migrate to the F−A interface is their ability to compensate for the excess of surface energy.[2,5] However, their migration during film formation is not straightforward. According to TEM images, film formation occurs from nonspherical colloidal particles, where F-containing entities exist as partial shells around p-MMA/nBA particles, and the length of the perfluoroalkyl side chain in each F-containing monomer affects the size of these domains. However, IRIRI as well as AFM data show that the majority of F-containing polymers are driven to the surface upon coalescence. Furthermore, the surface morphology depends on the molecular structure of the F-monomer utilized during synthesis. On the basis of these experiments, the following film formation mechanism is proposed in Scheme 1. As shown, film formation is initially dominated by p-MMA/nBA coalescence with the F-containing entities remaining intact at the surface of the particles. Upon further particle coalescence, the F-containing domains migrate to the F−A interface in efforts to compensate for the excess of surface free energy which is generated in the presence of p-MMA/nBA. This process leads to the formation of colloidal films with desirable F-containing moieties residing at the F−A interface. As shown in Scheme 1, the size of the generated domains is directly related to the molecular structure of the F-containing monomers. Specifically, for FBMA and FBA with short CF_2 entities, decreased packing efficiency and lower surface coverage is observed, but longer CF_2 chains results as possessed by FMA, FA, and FD results in films with increased packing efficiency and a larger surface coverage. This results in a larger degree of phase separation in the directions perpendicular to the F−A interface.

Conclusions

The utilization of a SDS/FSP surfactant mixture allows for the synthesis of colloidal dispersions containing various acrylic, methacrylic, and vinyl F-monomers. The presence of FSP surfactant significantly decreases the surface tension of the aqueous phase facilitating F-monomer diffusion during polymerization, thus producing nonspherical, monomodal colloidal particles possessing F-containing blocks near the exterior of the particles. The presence of each F-monomer in MMA/nBA colloidal systems results in a surface phase separation where longer perfluoroalkyl side chains produce larger

and more concentrated F-containing domains. Also, bulk film properties are affected by the side chain length where longer perfluoroalkyl functionalities results in tougher films while offering significant enhancements in chemical film stabilities.

Acknowledgment. The authors are thankful for support for these studies to the National Science Foundation Materials Research Science and Engineering Center (DMR 0213883). The authors are also thankful to the National Science Foundation I/U CRC Program under Award DMR EEC 0002775 for partial financial support of these studies.

References and Notes

(1) Dreher, W. R.; Jarrett, W. L.; Urban, M. W. *Macromolecules* **2005**, *38*, 2205.
(2) Eastoe, J.; Rankin, A.; Wat, R.; Bain, C.; Styrkas, D.; Penfold, J. *Langmuir* **2003**, *19*, 7734.
(3) Fasick, R.; Raynolds, S. E. I. DuPont de Nemours and Co., Pat. No. 3282905, 1966.
(4) Fasick, R.; Johnson, R. E. I. DuPont de Nemors Co., Pat. No. 3378609, 1968.
(5) Barthelemy, P.; Tomao, V.; Selb, J.; Chaudeir, Y.; Pucci, B. *Langmuir* **2002**, *18*, 2557.
(6) Borkar, S.; Siesler, H.; Hvilsted, S. *Macromolecules* **2004**, *37*, 788.
(7) Chen, Y.; Ying, L.; Yu, J. W.; Kang, E.; Neoh, K. *Macromolecules* **2003**, *36*, 9451.
(8) Cheng, S.; Chen, Y.; Chen, Z. *J. Appl. Polym. Sci.* **2002**, *85*, 1147.
(9) Huang, Z.; Shi, C.; Xu, J.; Kilic, S.; Enick, R.; Beckman, E. *Macromolecules* **2000**, *33*, 5437.
(10) Ha, J.; Park, I.; Lee, S.; Kim, D. *Macromolecules* **2002**, *35*, 6811.
(11) Kim, C. U.; Lee, J. M.; Ihm, S. K. *J. Appl. Polym. Sci.* **1999**, *73*, 777.
(12) Kostov, G.; Ameduri, B.; Boutevin, B. *J. Fluorine Chem.* **2002**, *114*, 171.
(13) Landfester, K.; Rothe, R.; Antonietti, M. *Macromolecules* **2002**, *35*, 1658.
(14) Linemann, R. F.; Malner, T. E.; Brandsch, R.; Bar, G.; Ritter, W.; Mulhaupt, R. *Macromolecules* **1999**, *32*, 1715.
(15) LoNostro, P.; Choi, S.; Ku, C.; Chen, S. *J. Phys. Chem. B* **1999**, *103*, 5347.
(16) Marion, P.; Beinert, G.; Juhue, D.; Lang, J. *Macromolecules* **1997**, *30*, 123.
(17) Marion, P.; Beinert, G.; Juhue, D.; Lang, J. *J. Appl. Polym. Sci.* **1997**, *64*, 2409.
(18) Munekata, S. *Prog. Org. Coat.* **1988**, *16*, 113.
(19) Yamana, M.; Uesugi, N.; Ogura, E. Daikin Industries, Ltd., Pat. No. 6126846, 2000.
(20) Parker, H.; Lau, W.; Rosenlind, E. S. Rohm and Haas Co., Pat. No. 6218464, 2001.
(21) Movchan, T.; Plotnikova, E.; Redina, L.; Gal'braikh, L.; Ys'yarov, O. *Colloid J.* **2003**, *65*, 47.
(22) Dargaville, T.; George, G.; Hill, D.; Whittacker, A. *Macromolecules* **2004**, *37*, 360.
(23) Deng, T.; Ha, Y.; Cheng, J.; Ross, C.; Thomas, E. *Langmuir* **2002**, *18*, 6719.
(24) Ding, L.; Olesik, S. *Macromolecules* **2003**, *36*, 4779.
(25) Gallyamoz, M.; Vinokur, R.; Nikitin, L.; Said-Galiyez, E.; Ernest, E.; Alexei, R.; Igor, V.; Schaumburg, K. *Langmuir* **2002**, *18*, 6928.
(26) Jin, J.; Smith, D.; Topping, C.; Suresh, S.; Chen, S.; Foulger, S.; Stephen, H.; Rice, N.; Nebo, J.; Mojazza, B. *Macromolecules* **2003**, *36*, 9000.
(27) Kang, S.; Luo, J.; Ma, H.; Barto, R.; Frank, C.; Dalton, L.; Jen, A. *Macromolecules* **2003**, *36*, 4355.
(28) Urban, M. *Attenuated Total Reflectance Spectroscopy of Polymers: Theory and Practice*; American Chemical Society: Washington, DC, 1996.
(29) Urban, M. *Encylcopedia of Analytical Chemistry*; John Wiley & Sons: New York, 2000.
(30) Otts, D. B.; Zhang, P.; Urban, M. W. *Langmuir* **2002**, *18*, 6473.
(31) ASTM Standard Test D 1894-01.
(32) Banks, R. E.; Smart, B. E.; Tatlow, J. C. *Organofluorine Chemistry Principles and Commercial Applications*; Plenum Press: New York, 1994.
(33) Morita, M.; Ogisu, H.; Kubu, M. *J. Appl. Polym. Sci.* **1999**, *73*, 1741.
(34) Aubrey, D.; Barnatt, A. *J. Appl. Polym. Sci.* **1968**, *6*, 241.
(35) Jones, A. *Macromol. Chem.* **1964**, *71*, 1.
(36) Shafrin, E.; Zisman, W. *J. Phys. Chem.* **1962**, *66*, 740.

MA050070W